Seismic performance of reinforced earth wall with geogrid

Comportement sismique d'un mur en sol armé de geogrille

A.Takahashi & J.Takemura – *Tokyo Institute of Technology, Meguro, Tokyo, Japan*
T.Shimodaira – *Taisei Corporation, Hyogo, Japan (Formerly: Tokyo Institute of Technology, Meguro, Tokyo, Japan*

ABSTRACT: This paper describes an experimental study on seismic performance of geogrid-reinforced vertical earth walls using a geotechnical centrifuge. Effects of length of geogrid and bulk density or compaction level of the soil on the seismic performance of the reinforced soil were discussed, especially on the permanent deformation of the soil when the reinforcement shows its effectiveness in preventing further deformation.

RÉSUMÉ: Cet article décrit une étude sur modèles centrifugés du comportement d'un mur de soutènement vertical renforcé par des nappes de géogrille. Les effets de la longueur des nappes, de la densité et du niveau de compactage du sol sur la réponse du mur armé sont analysés. Une attention est portée aux déformations permanentes du massif lorsque le renforcement montre son efficacité pour prévenir de nouvelles déformations.

1 INTRODUCTION

Geogrid-reinforced earth walls perform well against seismic forces, compared with other types of retaining structures. Although some displacements were observed in the reinforced earth walls in Hyogoken-nambu earthquake, no catastrophic failure took place even for the seismicity greater than the design value (e.g. Tatsuoka et al., 1997). This meant the importance of permanent displacement in the seismic design of geogrid-reinforced soil structure. In order to gain insight into the behaviour of geogrid-reinforced soil structures in earthquakes, a series of centrifuge model tests has been performed by the authors (Takahashi et al., 1998, 1999). In this study, centrifuge model tests were carried out on vertical geogrid-reinforced earth walls. Effects of length of geogrids and bulk density/compaction level of the soil on the seismic performance of the reinforced soil were discussed, especially on the permanent deformation of soil when the reinforcement shows its effectiveness in preventing further deformation of the reinforced soil.

2 TEST PROCEDURE AND CONDITIONS

2.1 *Test procedure*

TITech Mark II Centrifuge and servo-hydraulic type shaker were used in the tests (Takemura et al, 1989). Model setup used is shown in Fig. 1. During the tests, acceleration and displacement of the earth wall and tensile strains of the reinforcements were measured at the locations shown in Fig. 1. A lightweight aluminium model container with inner sizes of $450mm$ in width; $150mm$ in breadth and $250mm$ in height was used. Rubber sheets were placed at both side of the container for absorbing stress waves from the side boundaries.

Model geogrids used in the tests were a glass fibre made fly-guard, of which properties are listed in Table 1. Opening of the grids was $2.5 \times 2.5mm$. Inagi sand whose initial water content of 26–27% with dry density of $1.40/1.48Mg/m^3$ was used for making the model. Basic properties of Inagi sand are given in Table 2. Friction angle (ϕ) of the sand was obtained from triaxial compression tests under the drained condition. Cohesion (c) of the sand was back calculated from the failure height observed in a centrifuge test on non-reinforced vertical slope.

To investigate frictional interaction between the Inagi sand and the model geogrid, pull out tests were conducted. A typical test result of the pull out test is shown in Fig. 2.

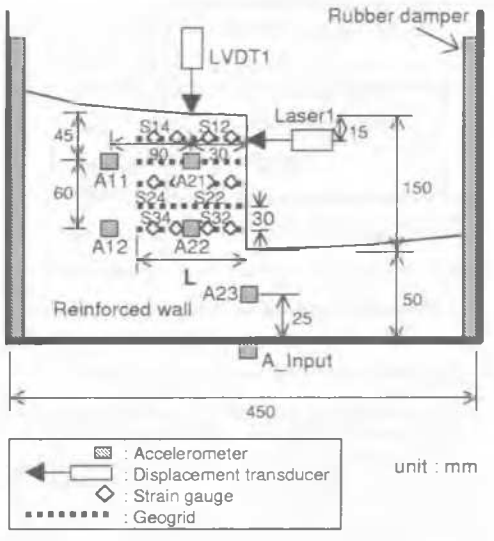

Figure 1. Model setup for centrifuge test.

Table 1. Material properties of model geogrid.

Mass per unit area	$1.1 \times 10^{-2}(0.56)kg/m^2$
Tensile strength T_f	$7.0(3.5 \times 10^2)kN/m$
Elongation at break ε_f	8.0 %

in parentheses, prototype scale

The area of contact between the geogrid and the soil was kept constant during the pullout test. The width (B) of the contact area was $148mm$ and the length (L) was $200mm$. The tensile strain of the geogrid when the pull out force reached its peak was about 0–3%.

In order to avoid the local failure at the vertical face of the wall, aluminium made facing plates were adopted as shown in Figs. 1 and 3. One piece of geogrid was attached to one plate, and these plates were connected in a hinged condition with each other as shown in Fig. 3. In the preparation of the model ground, Inagi sand with the initial water content of 26–27% was statically compacted in the model container to the dry density of $\rho_d = 1.40/1.48Mg/m^3$ layer by layer using a bellofram cylinder. The model geogrid was placed on each layer and optical markers for displacement

Table 2. Material properties of Inagi sand.

Specific gravity G_s	2.66
Mean grain size $D_{50}(mm)$	0.20
Uniformity coefficient U_c	3.2
Modulus of deformation $E_{50}(kPa)$	$1.0 \times 10^{3*}$, $2.6 \times 10^{3**}$
Cohesion $c(kPa)$	4.2^*, 6.8^{**}
Internal friction angle ϕ (deg.)	33^*, 35^{**}

* $\rho_d = 1.4Mg/m^3, w_0 = 27\%$, ** $\rho_d = 1.48Mg/m^3, w_0 = 26\%$

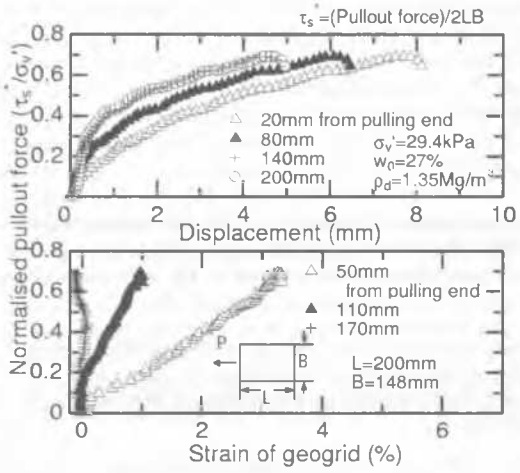

Figure 2. Typical pull-out test result.

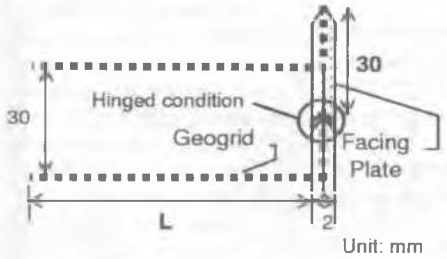

Figure 3. Schematic drawing of model facing plates.

Table 3. Applied sinusoidal waves of each step.

Step	Amplitute (G)	Number of waves
1st	10 (0.2)	20
2nd	15 (0.3)	20
3rd	20 (0.4)	20
4th	20 (0.4)	40

in parentheses, prototype scale

measurement were also placed at the front surface of the ground. This compaction was continued up to the top level of the earth wall. Having prepared the model, the container was set on the shaking table mounted on the centrifuge. Shaking tests were conducted under $50G$ centrifugal acceleration by inputting sinusoidal waves with a frequency of $100Hz$, which is equivalent to $2Hz$ in the prototype scale, to the shaking table. Four waves with different conditions shown in Table 3 were input to each model. Typical time histories of the input sinusoidal waves are shown in Fig. 4 in the prototype scale. Photographs were taken before and after shaking to observe the displacement of targets on the front surface of the reinforced soil.

2.2 *Test conditions*

Table 4 gives the test conditions adopted in this study. The height of the reinforced soil wall was $150mm$, $7.5m$ in the prototype scale. The spacing between geogrids was $30mm$, $1.5m$ in the prototype scale. Effects of the length of geogrids (L) and the dry density of the soil (ρ_d) on the permanent deformation of soil, when the reinforcement shows its effectiveness in preventing further deformation of the reinforced soil, were investigated. Factors of safety calculated by the

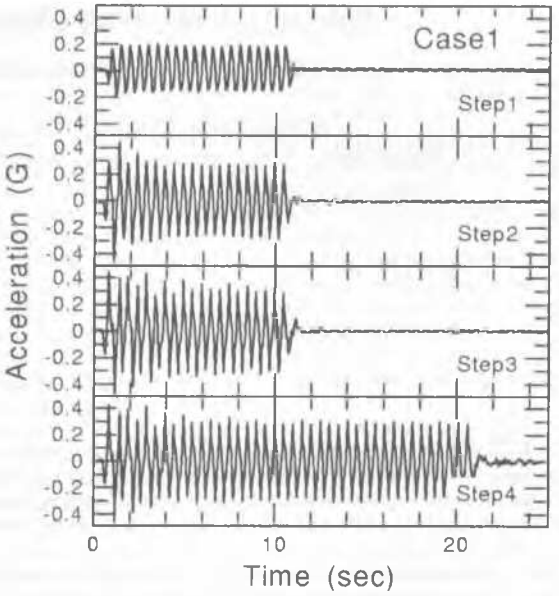

Figure 4. Input waves time histories (Case1).

Table 4. Test conditions.

Test case	$\rho_d(Mg/m^3)$	L (mm)	Safety factor at $k_h = 0.2$
0	1.48	40 (2000)	0.89
1	1.48	120 (6000)	1.58
2	1.40	120 (6000)	1.48
3	1.48	90 (4500)	1.36
4*	1.40	90 (4500)	1.27

in parentheses, prototype scale
* strain gauges were not attached on the grids

modified Fellenius method against the horizontal seismic coefficient of 0.2 are listed in Table 4. The factors were not sensitive to the variation of the bulk density of the soil. Before shaking tests, natural frequency of the reinforced soil was measured using random wave with small intensity. It was found that the natural frequencies of the wall were $180Hz$ in Case 1 and $140Hz$ in Case 2, respectively. These correspond to $3.6Hz$ and $2.8Hz$ in the prototype scale.

3 TEST RESULTS AND DISCUSSION

All data presented in this section are in prototype scale.

3.1 *Permanent deformation of earth walls*

Incremental and total permanent horizontal displacements of the wall faces at the height of $6.75m$ (Laser1) and incremental and total settlements of the walls at the shoulder of the wall (LVDT1) for each shaking step are shown in Fig. 5. The accumulation of the permanent displacements became larger, as the length of the geogrids and the dry density of the soil decreased. In the Cases 1–4, incremental permanent displacement in each shaking decreased with the shaking number, while they increased with the shaking number in Case 0, whose length of the geogrid was the shortest among all the tests.

Observed deformation of the walls after 4th shaking step are shown for Cases 0, 3 & 4, respectively in Fig. 6. In Case 0 with the shortest length of geogrids, the failure mode was circular type and the failure line was across the geogrid-reinforced zone at the lower portion of the wall. Except Case 0, observed deformation mode of the reinforced soil was a two-part wedge type and relatively large deformation was observed at the lower portion of the wall, although the magnitude of displacement differs for different conditions. The permanent deformation modes of the walls in Cases 1 & 2 were essentially the same as observed in Cases 3 & 4.

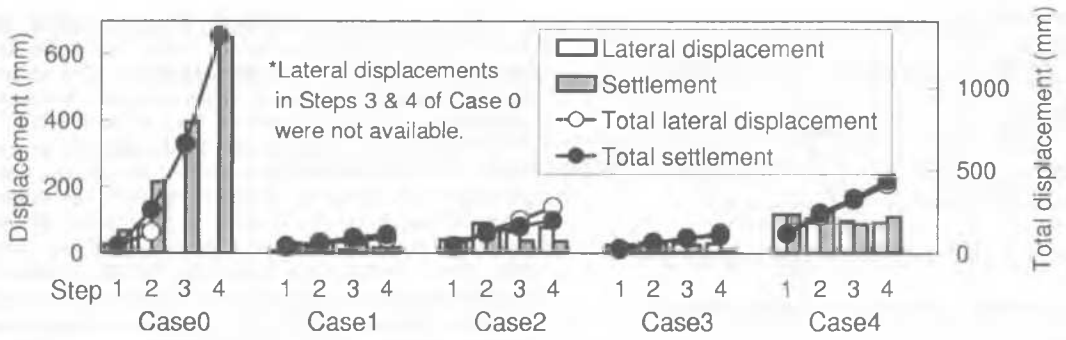

Figure 5. Permanent displacement of the walls (Cases 0–4).

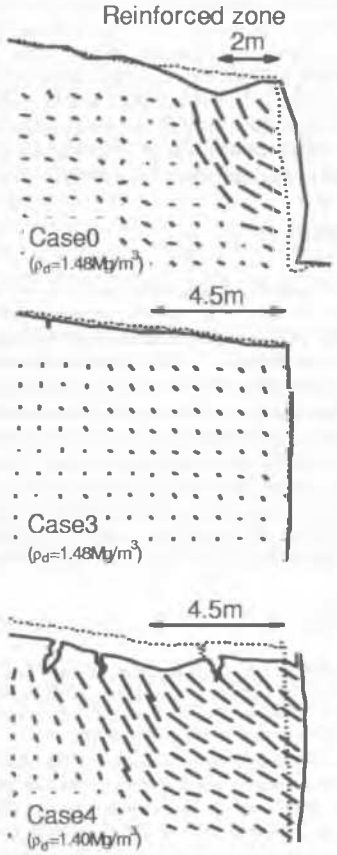

Figure 6. Permanent deformation of the walls (Cases0, 3 & 4, Step4).

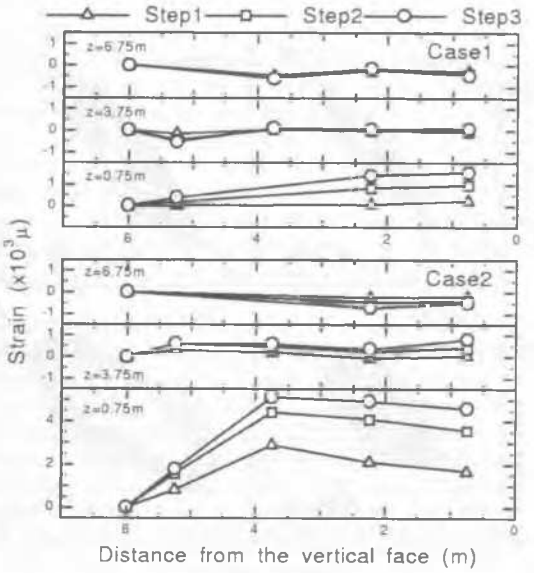

Figure 7. Residual strain of geogrids (Cases1 & 2, Step1–3).

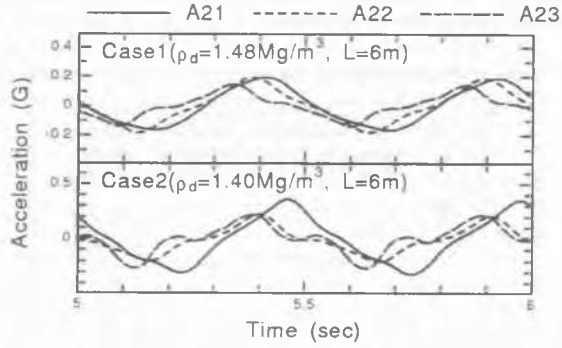

Figure 8. Acceleration time histories (Cases1 & 2, Step2 at A21, A22 & A23).

Observed distributions of the residual strain of geogrids at the different elevations; $z = 6.75, 3.75\&0.75m$, for each step of Cases 1 & 2 are shown in Fig. 7. Positive values in the figure represent elongation of the grids. Irrespective of the bulk density of the soil, the larger residual strain of geogrids was observed at the lower portion of the wall, compared to the upper portion. Paying attention to the accumulation of the residual strain of the grids at the lower portion, a large strain was observed along the geogrid in the first step for the case with a small soil density; Case 2, while in Case 1 with a large density, the residual strain in the first step was very small and gradually increased backward from the face with the following shaking number. This tendency is probably associated with the progress of the permanent deformation of the wall and indicates that the slight lack of the compaction of the soil results in the large permanent deformation of the wall.

3.2 *Acceleration responses and stress–strain relationships of reinforced soils*

Figure 8 shows partial time histories of the acceleration at A21, A22 & A23 in Step 2 for Cases 1 & 2. The points of A21 & A22 were located in the reinforced zone and the point of A23 was in the base. The phase lag between the acceleration of A21 and A22 in Case 2 was larger than that in Case 1. This fact implies that the relatively large deformation of the reinforced zone occurred in Case 2 whose dry density of the soil was smaller than that in Case 1. This difference is induced by not only the natural frequency of the reinforced soil wall, but also the deformation characteristic of the wall.

Generally, the effect of the reinforcement can be seen when the tensile strains of the geogrid increase with the deformation of the reinforced soil. To gain insight into the relationship between the effect of the reinforcement and the deformation of the soil, mean stress–strain relationships of the reinforced zone were calculated from the acceleration records. The applied method for stress–strain calculation was proposed by Koga et al. (1990) and was briefly summarised in Fig. 9. The used acceleration records were mea-

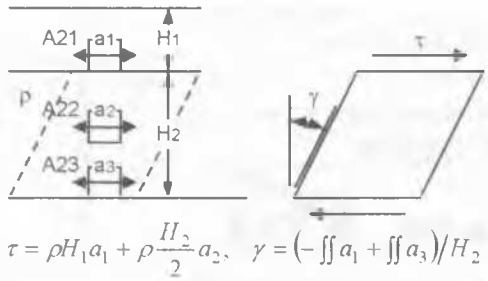

Figure 9. Calculation of shear stress and strain from acceleration records.

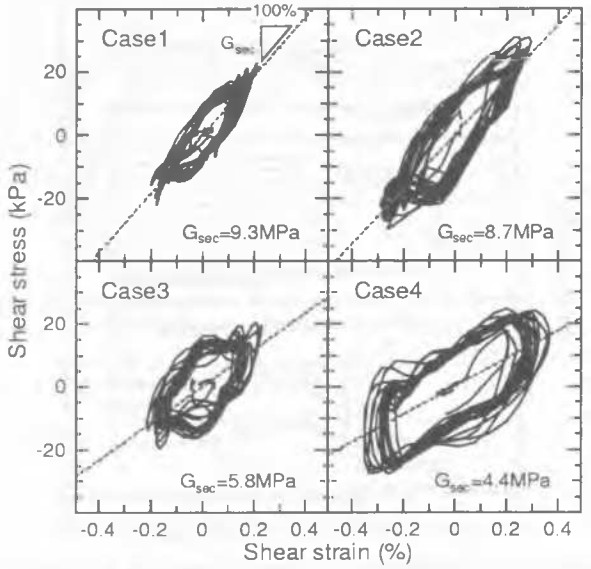

Figure 10. Relationship between shear stress and strain of reinforced zone (Cases1–4, Step3).

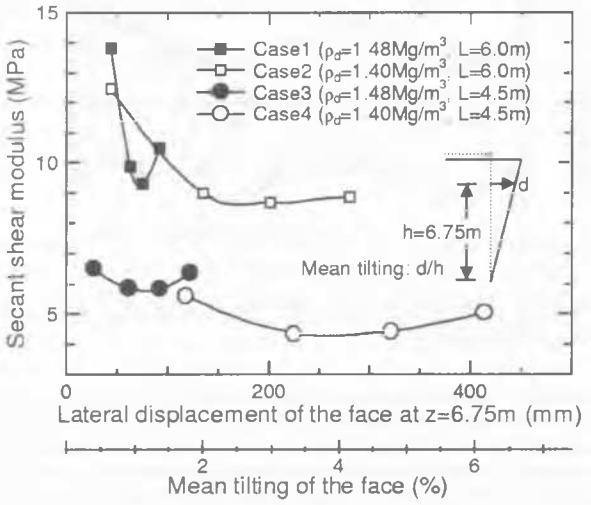

Figure 11. Variation on shear modulus with lateral displacement of the facing.

sured at A21, A22 & A23. The records were filtered by cutting out frequencies of less than $0.4Hz$ and greater than $10Hz$, thus no residual strain was included in the results. The calculated stress–strain relationships of the third shaking step are shown in Fig. 10 for Cases 1–4. From the stress–strain relationships, it can be found that the secant shear modulus becomes larger and the amplitude of strain becomes smaller, as the length of geogrids and the dry density of the soil increase.

The secant shear moduli shown in the figure were the slopes of the approximated line of stress–strain relations calculated by the least squares method. The secant shear moduli are plotted against the permanent horizontal displacements of the wall face at the height of $6.75m$ in Fig. 11. Additional horizontal axis in the figure represents the mean tilting of the wall face defined by the horizontal displacement at the $6.75m$ height divided by the height. This mean tilting of the wall can be a good index of the mean shear strain of the reinforced zone. In all the cases, once the secant shear moduli decreased with the permanent lateral displacement of the soil wall. However the secant shear modulus increased, when the permanent displacement of the soil reached a certain level in all the cases. These turning points in the variation of the shear modulus with the displacement of the reinforced soil should be the points that the strained reinforcement showed its effectiveness in preventing the further deformation of the wall. These points varied according to the compaction level of the soil. The mean shear strains of the reinforced soil at the turning point were about 1% in the cases of the well-compacted wall and 3–4% in the cases of the small bulk density, even though the difference of the dry density was 5%.

4 CONCLUSIONS

Effects of the length of geogrids and dry density or compaction level of the soil on the seismic performance of the reinforced soil were experimentally investigated in the geotechnical centrifuge. The accumulation of the permanent displacements of the wall in earthquakes became smaller as the length of the geogrids increased. It was confirmed that the compaction of soil was of critical importance for the reinforced earth structure. Several percent differences in the dry density of the soil induced the several fold difference in the mean shear strain of the reinforced soil at which the reinforcement can be efficiently mobilised against the larger deformation of the soil structure.

REFERENCES

Tatsuoka, F., Koseki, J. & Tateyama, M. 1997. Performance of reinforced soil structures during the 1995 Hyogo-ken Nambu Earthquake. *Proceedings of the international symposium on earth reinforcement*, Vol. 2, 973-1008.

Takahashi, A., Takemura, J., Tsutsumi, F. & Sae-Tia, W. 1998. Shaking table tests on geogrid-reinforced embankment during earthquake with centrifuge. *Proceedings of 10th Earthquake Engineering Symposium*, Vol. 2, 1551-1556 (in Japanese).

Takahashi, A., Takemura, J. & Izawa, J. 1999. Dynamic behavior of vertical geogrid-reinforced soil during earthquake, *Proceedings of the International symposium on Slope stability engineering*, Vol.2, 991-996.

Takemura, J., Kimura, T., & Suemasa, N. 1989. Development of Earthquake simulators at Tokyo Institute of Technology. Technical Report, No. 40, Dept. Civil Engrg. Tokyo Institute of Technology, 41-60.

Koga, Y. & Matsuo, O. 1990. Shaking table tests of embankments resting on liquefiable sandy ground, *Soils and foundations*, Vol. 30, No. 4, 162-174.